Journal of Nuclear Materials 384 (2009) 249–255

Contents lists available at ScienceDirect

Journal of Nuclear Materials

journal homepage: www.elsevier.com/locate/jnucmat

Nano-cavities observed in a 316SS PWR flux thimble tube irradiated to 33 and 70 dpa

D.J. Edwards [a], F.A. Garner [a,*], S.M. Bruemmer [a], Pål Efsing [b]

[a] Pacific Northwest National Laboratory, MS P8-15, P.O. Box 999, Richland, WA 99354, Unites States
[b] Vattenfall AB Ringhals, SE-430-22 Väröbacka, Sweden

ARTICLE INFO

Article history:
Received 11 June 2008
Accepted 20 November 2008

ABSTRACT

The radiation-induced microstructure of a cold-worked 316SS flux thimble tube from an operating pressurized water reactor (PWR) was examined. Two irradiated conditions, 33 dpa at 290 °C and 70 dpa at 315 °C were examined by transmission electron microscopy. The original dislocation network had completely disappeared and was replaced by fine dispersions of Frank loops and small nano-cavities at high densities. The latter appear to be bubbles containing high levels of helium and hydrogen. An enhanced distribution of these nano-cavities was found at grain boundaries and may play a role in the increased susceptibility of the irradiated 316SS to intergranular failure of specimens from this tube during post-irradiation slow strain rate testing in PWR water conditions.

1. Introduction

As operating light water cooled nuclear power plants (LWRs) approach their design lifetimes of 40 years, there is increasing interest in extending their licenses to 60 years. In order to support such extension, it is necessary to provide data that confirms the projected structural integrity of important core components at higher exposures. An important example is the austenitic stainless steel, baffle-former-barrel assembly that surrounds the core of a pressurized water reactor (PWR) [1].

The majority of these internal components are constructed from AISI 304SS and to lesser extent from AISI 316SS. Unfortunately, microstructural and mechanical data at PWR-relevant irradiation conditions are not available at sufficiently high neutron exposure. It is considered to be impractical to remove sections of the baffle-former-barrel assembly of an operating reactor for destructive examination in order to provide the required data.

At 60 years, some near-core locations in PWR internal components can reach exposures greater than 100 dpa. While data on stainless steels at such dpa levels are available from previous fast reactor irradiations, damage was produced at much higher temperatures and dpa rates than are characteristic of PWR internals. Additionally, there is a significant difference in neutron spectra with strong consequences on transmutation, especially as related to production of helium and hydrogen.

One way to obtain PWR-relevant data at higher exposures is to remove a more accessible component from inside of the core where the dpa rates are approximately two to three times higher. Flux thimble tubes are used to measure the neutron flux-spectra in the core center and are often resident in core for one or more decades. These tubes are easily removed and sectioned to provide specimens for various destructive tests.

This paper examines the microstructure of a thimble tube removed from a currently operating European PWR. Some of the experimental results presented in this paper were published in less detail earlier [2]. This thimble was sectioned to produce a number of segments to be distributed to European, American and Japanese participants. Earlier reports on two other studies using these tube segments provide data on corrosion behavior and changes in mechanical properties [3,4].

2. Experimental details

The thimble tube was constructed from 15% cold-worked 316SS and was removed during an outage in 1998. The tube was 7.65 mm in outside diameter with 1.22 mm thickness. It had been in service for 23 years before removal, accumulating 15.9 effective full power years of operation.

The tube's composition was Fe-13.3Ni-17.4 Cr-2.69Mo-1.70Mn-0.43Si-0.045C-0.026P-0.010S-0.044N, as determined from archive vendor qualification documents. No unirradiated archive specimen was available for comparison, but a section of the tube removed from a position well below the core was available at essentially zero dose.

The tube was in contact with water coolant pressurized at 2250 psi (15.5 MPa), and extended from the top of the core to a penetration in the lower head of the reactor pressure vessel. It experienced temperatures ranging from 290 °C at the bottom to 325 °C well above the top of the core, reaching a maximum dose

* Corresponding author. Tel.: +1 509 376 4136; fax: +1 509 376 0418.
E-mail address: frank.garner@pnl.gov (F.A. Garner).

0022-3115/$ - see front matter © 2008 Elsevier B.V. All rights reserved.
doi:10.1016/j.jnucmat.2008.11.025

of 70 dpa at 321 °C. The temperature of the tube at any elevation in core is within 1 °C of the local water temperature.

In this study, TEM discs for electron microscopy were prepared from different sections of the tube by cutting a thin strip from a section of the tube and mechanically grinding the specimen to a thickness to ~0.125 mm. One set of microscopy specimens were obtained from the peak exposure position in the top half of the reactor core (~0.6 m from the top), with a dose, dose rate and irradiation temperature at this location calculated to be ~70 dpa, $\sim 1 \times 10^{-7}$ dpa/s and 315 °C. A second set of microscopy specimens was obtained from a section near the bottom of the reactor core (~3.7 m) at ~33 dpa, $\sim 0.5 \times 10^{-8}$ dpa/s and 290 °C.

The specimens were electrolytically thinned using a Tenupol 3 jet-polishing unit at 20 °C, 65 mA and 38 volts in an electrolyte of 5% perchloric acid and 95% acetic acid. The microstructure was examined in a 2010F field-emission-gun TEM operating at 200 kV. Microstructural characterization involved imaging dislocations, deformation twins, small dislocation loops and cavities, and then measuring their size and density. Thickness measurements were obtained from the examined regions using convergent beam electron diffraction at the same diffraction condition and tilt as used to image the Frank loops. Nominal thicknesses of the foil regions used for defect and cavity measurements were around 55–70 nm.

3. Results

The grain structure of both irradiated specimens was found to be equiaxed with a limited density of twins. No remaining dislocation structure associated with the cold working was found in either the 33 or 70 dpa specimens. Replacing the dislocations were a high density of Frank loops and a high density of nano-cavities. No precipitates were observed at 33 dpa but some evidence of a low density of small precipitates was observed in bright-field images at 70 dpa, but the precipitates did not produce any visible diffraction spots. Attempts to blind-image these precipitates by placing the aperture over known precipitate reflections did not yield a conclusive answer, indicating that such small precipitates were too few and too small to generate a dark-field image.

The Frank loops were isolated from the rest of the microstructure by the use of centered dark-field imaging. This was accomplished by tilting to an <0 1 1> zone axis and then tilting the foil to a **g**1 1 3 2-beam condition. At this orientation, two sets of streaks in the [1 1 1] directions arose via electron diffraction from the stacking fault of each loop; the larger and higher the density of the Frank loops, the brighter the streaks. One set of these streaks, corresponding to a single variant of the four possible variants, was tilted to produce a centered dark-field condition that highlighted the stacking fault of each Frank loop down to sizes less than 1 nm. The measured loop densities were multiplied by 4 to account for the three missing variants. It was assumed that the distribution on the four close-packed planes were identical, an assumption that is only correct in the absence of imposed shear stresses [5,6]. Although no loop distributions have been measured previously for fully compressive stress states such as experienced by this tube, the theory developed to describe loop distributions is equally applicable to zero, positive or negative hydrostatic stress states [5]. Examples of the Frank loops are shown in Fig. 1, and the size distributions of Frank loops are presented in Fig. 2. The shapes of the loop size distributions are similar for the two specimens, but loops at the higher temperature condition (70 dpa/315 °C) had a density lower by a factor of two and a slightly larger average size than that of the 33 dpa/290 °C condition. A summary of the loop densities is provided in Table 1.

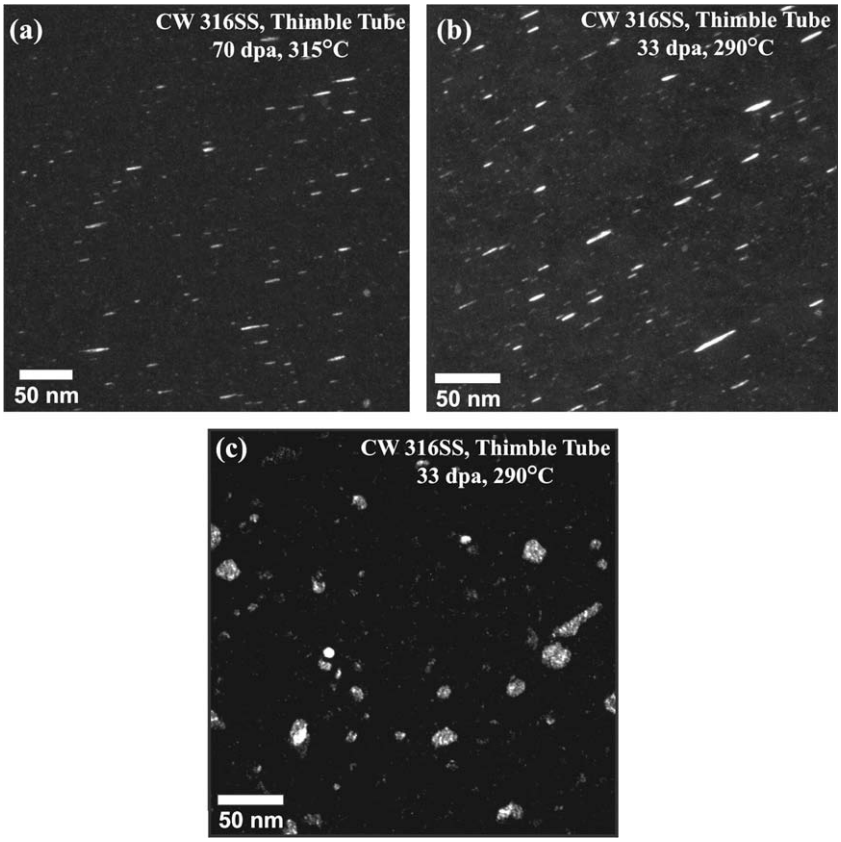

Fig. 1. Examples of Frank loops at (a) 70 dpa, 315 °C and (b) 33 dpa, 290 °C as observed edge-on on one set of the four (111) planes using the dark-field relrod technique. The image in (c) is from Frank loops inclined to the beam direction imaged using a relrod in the diffraction pattern.

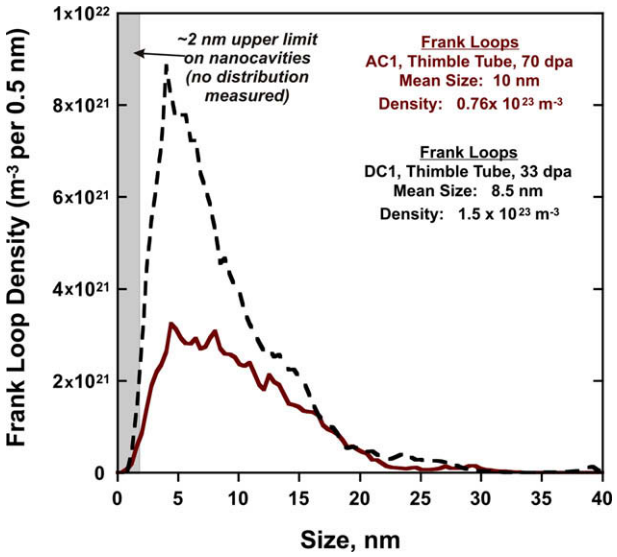

Fig. 2. Comparison of measured size distributions of Frank loops for the two irradiation conditions. The size range of the nano-cavities is shown for comparison.

The most significant observation was the very high density of nano-cavities found in both irradiation conditions (see Table 1). These cavities were much more noticeable in the 70 dpa/315 °C condition because their density was significantly higher and their average size slightly larger than observed in the lower-temperature, lower-dose condition. A somewhat higher density of cavities was present at grain boundaries in both conditions, an example of which is shown in Fig. 3.

Some indication of a denuded zone appears on each side of grain boundaries in the 70 dpa/315 °C condition, suggesting that the cavities were enhanced at the grain boundary at the expense of adjacent matrix. On one grain boundary in the 70 dpa/315 °C sample, the linear spacing between cavities was estimated to be ~10 nm within the boundary plane based on measurement of areal densities. The cavities on the grain boundaries appear to be somewhat smaller than their counterparts in the alloy matrix.

The nano-cavities in both the matrix and at the grain boundaries reside in a size range (1–3 nm) that is difficult to reliably quantify without the use of image simulations. The cavity images are very sensitive to the under-focus condition used, as shown in Fig. 4. Using an under-focus condition of 768 nm enhances the Fresnel fringe around each cavity boundary to the extent that the individual cavity images overlap. Using a lower under-focus condition of 128–256 nm, the nano-cavities were in fact found to be well separated.

Another problem encountered with imaging of the small cavities was that electropolishing introduced a surface artifact that showed up distinctly when the image is under-focused at high magnification. The artifact is not thought to arise from surface contamination, but appears to be some type of very fine, nano-scale etching that obscures the contrast of the smallest cavities. To compensate for this complication, it was necessary to scrutinize each cavity-like image to discern between surface etches and real cavities. Thus the cavity densities listed in Table 1 are thought to be underestimates of the actual densities, and likewise, the average size is probably lower than specified. If surface etchings are unrecognized as such, however, it is possible to overestimate the cavity density by including etchings and real cavities.

Table 1
Summary of microstructural characteristics.

Irradiation conditions	Loop density (10^{23} m^{-3})	Mean loop size (nm)	Precipitate density (10^{23} m^{-3})	Mean precipitate size (nm)	Cavities (10^{23} m^{-3})
33 dpa 290 °C	1.5	8.5	–	–	0.61
70 dpa 315 °C	0.76	10	<10^{21}	~10	1.6 size <3 nm

4. Discussion

The high density of Frank loops observed was expected for these irradiated stainless steels, but the lack of line dislocations observed in the initially cold-worked material was somewhat surprising. In a companion study [7] on this same thimble tube, a specimen removed from a non-irradiated section well below the core (~4.8 m) at 290 °C showed that the microstructure was comprised of a evenly-distributed, tangled dislocation network consistent with 15% cold work. The retention of this microstructure for ~23 years at 290 °C attests to the durability of the dislocation network against thermally-induced relaxation, but its absence by 33 dpa at the same temperature indicated that radiation-induced displacements and the concurrent radiation-enhanced diffusion prove very effective at removing the network of dislocations.

As discussed in Ref. [2], loop microstructures observed in these specimens agree very well with those of fast reactor specimens, as well as with those reported by others on PWR thimble tubes [3,8], with only minor differences in distribution at comparable irradiation conditions. The nearly complete radiation-induced loss of the cold-worked line dislocation network is also a very general observation.

The nano-cavities observed in this study are assumed to be gas-filled bubbles. For the 33 and 70 dpa specimens examined in this study, however, no gas measurements were made. However, the gas-filled nature is supported by the measurements of Fujimoto and coworkers [3] on this same thimble tube but at a slightly different location. At 65 dpa and 320 °C for example, helium was measured to be ~625 appm and hydrogen to be ~2100–2400 appm. The helium concentration at 70 dpa should be larger than that at 65 dpa on the same tube and it is reasonable to assume that the hydrogen level will be comparable and perhaps larger.

Fig. 5 shows Fujimoto's measurements of these gases along the thimble tube after 15.9 effective full power years as a function of dpa level. Also shown are data from another thimble published by Fujii and coworkers [8], derived from two Japanese PWR thimble tubes irradiated to exposures of 9 and 13 effective full power years. The helium content of the tube found in Fujimoto's studies is observed to climb continuingly with increasing dose. Since the helium is generated primarily via thermal neutrons and the dpa level primarily via fast neutrons it is expected that variations of thermal/fast neutron ratio, especially near the core edges, will induce some variations in helium generation rate vs. dose rate when measured on a single tube.

Most importantly, the retained hydrogen was measured by Fujimoto to climb as the helium level increased, but to decrease somewhat at the highest dose. At these gas concentrations and considering the very high cavity density, it is thought that a very large fraction of both gases must reside inside of the nano-cavities rather than in the matrix.

The maximum hydrogen level of ~2500–3300 appm measured by Fujimoto in this thimble tube is rather large compared to the 100–300 appm usually observed in stainless steels irradiated to lower neutron exposures in BWRs [9]. As a consequence of the hydrogen overpressure maintained in PWRs, the retained hydrogen levels are usually somewhat higher at 400–600 appm [10].

It was previously thought that hydrogen could not be stored in stainless steels above levels of several 100 appm. Garner and coworkers [11] have demonstrated, however, that significant

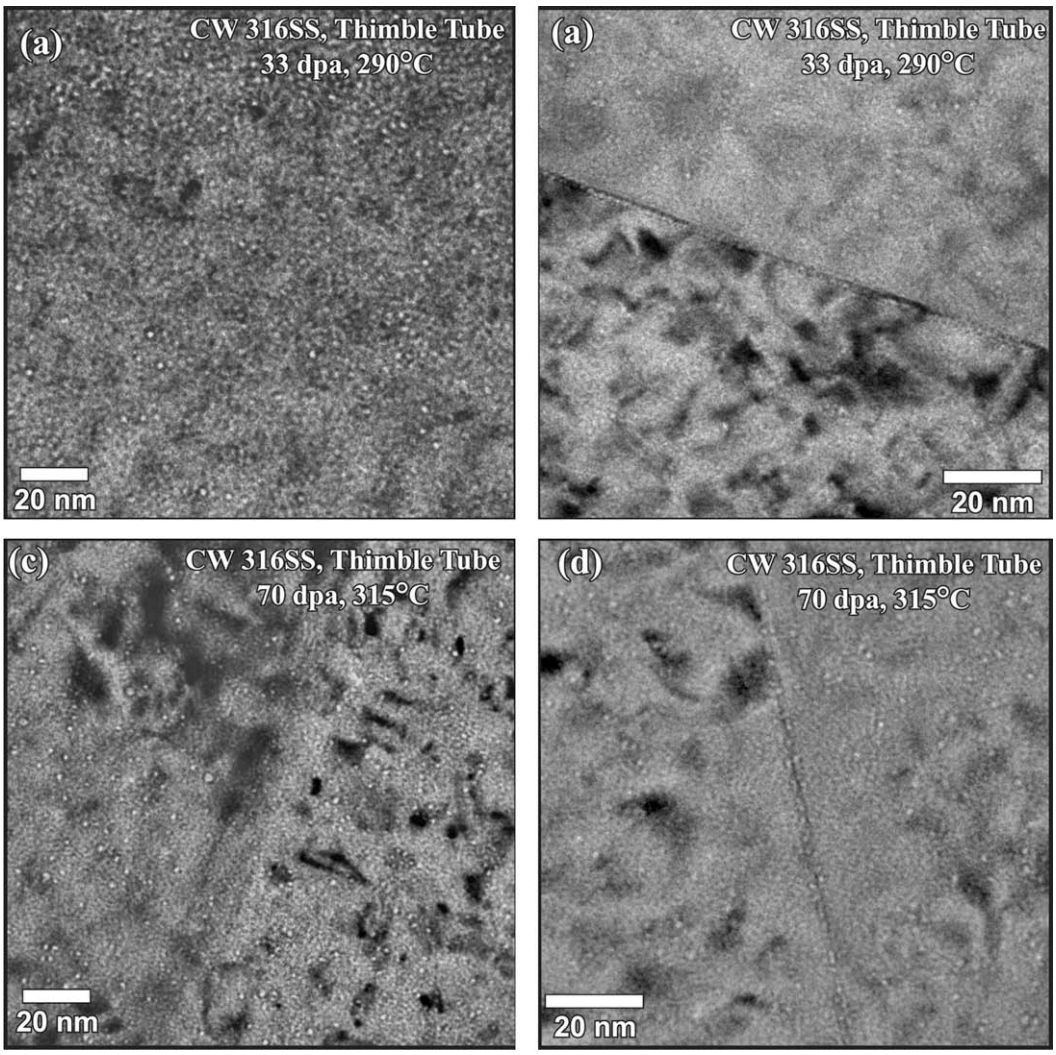

Fig. 3. Images of nano-cavities in the thimble tube at conditions (a-b) 33 dpa, 290 °C and (c-d) 70 dpa, 315 °C. (-256 mm under-focus condition).

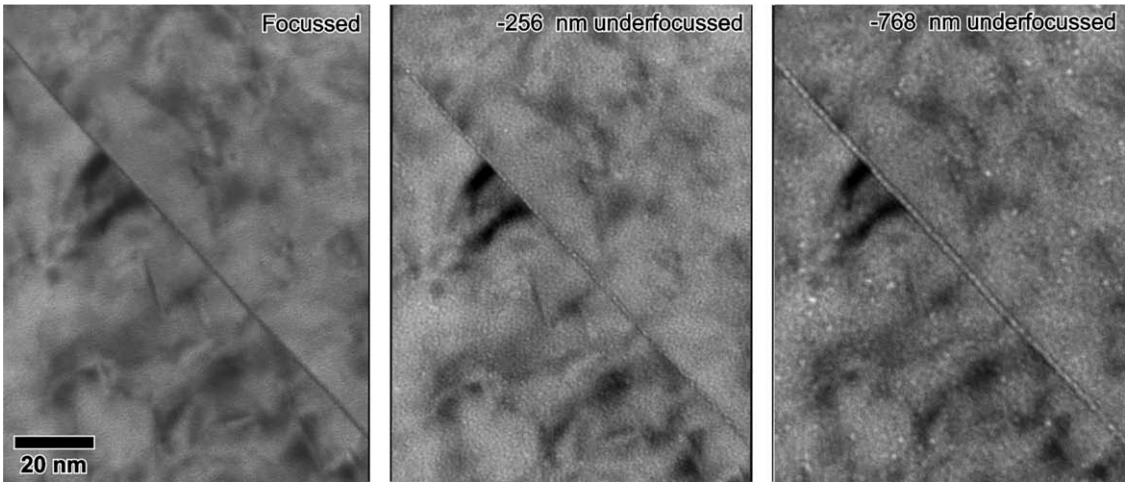

Fig. 4. Images demonstrating the sensitivity of nano-cavity images to the focus condition.

amounts of hydrogen in excess of that predicted by Sievert's Law can be stored in irradiated steels and pure nickel when cavities nucleated by helium begin to form at high densities. They postulate that hydrogen is most likely stored inside the cavities rather than on the cavity surfaces or in the intervening matrix. They also note that hydrogen found to be stored in the cavities is produced not only by transmutation but also arises from a number of environmental sources associated with the presence of water. In some cases the retained hydrogen was shown to exceed that produced by transmutation.

The transmutation sources of both helium and hydrogen in BWR and PWR spectra are primarily the 'double-nickel' thermal neutron sequences, $^{58}Ni(n,\gamma)$ $^{59}Ni(n,\alpha)$ and $^{58}Ni(n,\gamma)$ $^{59}Ni(n,p)$, and secondarily from high energy (n,γ) events with all five nickel isotopes [10–14]. Therefore the production rates are proportional to the nickel content and to the thermal-to-fast neutron ratio. The latter varies across the length of the tube, especially just outside the upper and lower core boundaries.

It is important to recognize that the double-nickel sequence produces nonlinear buildups of helium and hydrogen since it is necessary to first produce the non-naturally occurring ^{59}Ni isotope before the gas production reactions can operate strongly. Therefore, the helium/dpa and hydrogen/dpa production rates increase with time or exposure at a given core elevation.

As shown in Fig. 6 there is a bump in the helium/dpa ratio at ~3 dpa in Fujii's measurements that reflects a similar peak in the thermal neutron population that exists just outside the core boundaries [10]. No data are available at a comparable position in the studies of Fujimoto.

At this time, however, we are unable to offer an explanation of why the hydrogen levels in Fujii's study do not climb with fluence but remain in the 400–600 appm range associated with PWRs with hydrogen overpressure. This study involved a different heat of steel in a different reactor with possibly different operational history, but insufficient information is available to attempt to rationalize the difference in hydrogen production in the two studies.

While the changes in helium and He/dpa level with increasing residence time are consistent with expectations based on nonlinearity of helium production, the changes in hydrogen and H/dpa level are rather dramatic, especially in Fujimotos's study. This difference supports the arguments of Garner and coworkers [11] that require helium-nucleated cavities to first form before signifi-

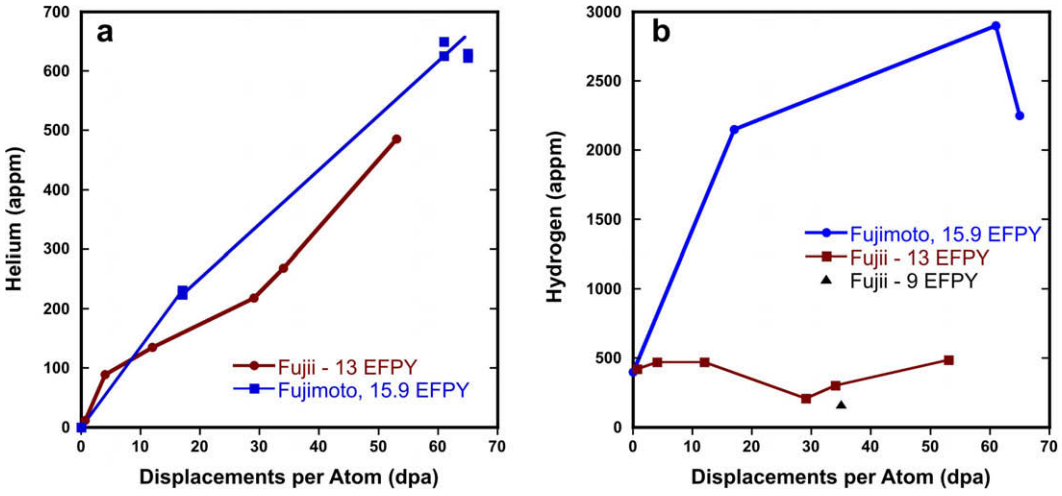

Fig. 5. Measurements of (a) the average helium and (b) the average hydrogen concentrations in the thimble tube as measured by Fujimoto [at 15.9 effective full power years [3] and also by Fujii [8]. Times are given in effective full power years, not total years.

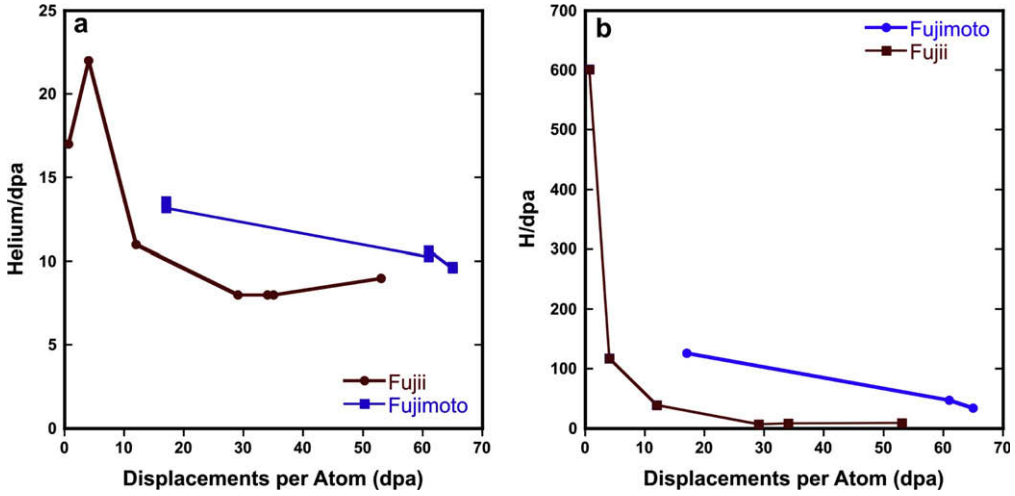

Fig. 6. Calculated gas generation rates per dpa for studies conducted by Fujimoto and Fujii.

cant co-storage of hydrogen can occur. Once some threshold of helium-nucleated cavity volume is reached, hydrogen from both transmutation and environmental sources can then be stored. Thus, we are seeing a strongly nonlinear increase in hydrogen storage between 9 and 13 EFPY and 15.9 EFPY of reactor operation. Unfortunately this interpretation is not fully convincing since Fujii clearly demonstrated that nano-cavities were present in his specimens.

Consistent with the results of our study Fujii also showed that the nano-cavities required significant under-focus conditions in order to be visible. In Fujii's case an under-focus of −1200 nm was used to image the cavities and measure their sizes.

A major question is whether there are any consequences to the nano-cavity development along grain boundaries and local storage of helium and hydrogen. As shown in Fig. 7 Fujimoto et al. [3] discovered an increasing susceptibility to intergranular (IG) failure in PWR primary water and in argon during post-irradiation slow strain rate tests conducted on specimens removed from this same thimble tube. Essentially 100% IG stress corrosion cracking (SCC) was observed at doses greater than ~40 dpa. Significant IG cracking was also observed when tests were conducted in argon gas. This response is consistent with results of earlier work by Fukuya and coworkers [15].

Fujimoto suggested that the higher susceptibility to IG fracture arose as a consequence of helium and hydrogen-filled bubbles decorating the boundaries. He noted that specimens irradiated to comparable dpa levels in contact with sodium coolant in the BOR-60 fast reactor was much less susceptible to IGSCC when tested in PWR water conditions. Significantly with respect to the hypothesis proposed in this paper concerning He and H effects, the gas levels produced were very much lower in the BOR-60 specimens. Indeed, Edwards and coworkers did not find bubbles of any size in stainless steel specimens irradiated at similar temperatures and doses in BOR-60 [2].

Garner et al. [11,14] has shown that specimens irradiated in fast reactors indeed produce lower levels of helium and hydrogen per dpa, but they also showed that hydrogen produced by both environmental and transmutation sources is lost from fast reactor specimens by partition to the sodium. Therefore, hydrogen storage does not occur in stainless steels after fast reactor irradiation.

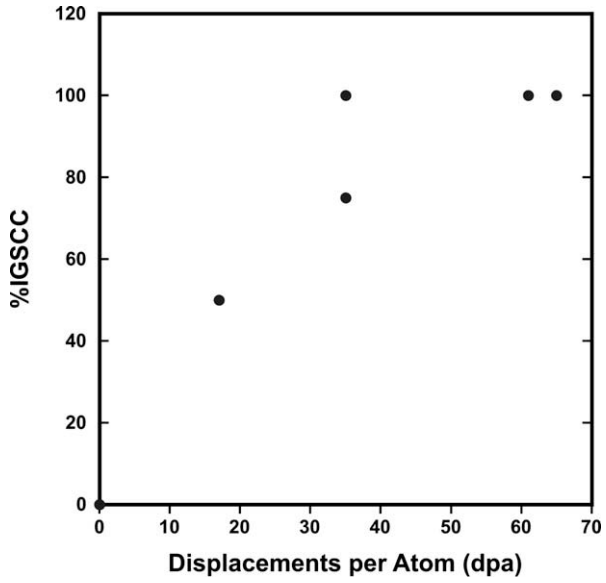

Fig. 7. %IGSCC measured by Fujimoto developed during slow strain rate tests conducted on the thimble tube examined in this study [3].

The observation of nano-cavities in PWR-irradiated stainless steels is not unprecedented. In addition to the study of Fujimoto, Fujii and coworkers [8] reported observing such cavities in a similar study conducted on two thimble tubes removed from a Japanese PWR after 9 and 13 effective full power years. The dose rates varied from 0.02 to 1.3×10^{-7} dpa/sec with doses ranging from 1 to 53 dpa and temperatures between 290 and 320 °C, conditions that are almost identical to those of this study. They reported a cavity density of 6.9×10^{23} m^{-3} at 31 dpa and 290 °C, which is roughly a factor of 4 higher than found in this study. They did not find bubbles with sizes above ~2 nm, whereas our study shows a small fraction of the bubbles extend up to 3 nm in diameter. One significant difference relative to the current study is that while the 486 appm He at 53 dpa is comparable to the ~600 appm observed at 70 dpa in the Fujimoto study, the hydrogen observed by Fujii was ~488 appm, considerably lower than the ~2500 appm measured by Fujimoto.

A study by Foster and coworkers [16] studied the microstructure of another thimble tube irradiated for 11 effective full power years to ~35 dpa at temperatures at 310 °C. Helium and hydrogen levels were not measured and they did not report the Frank loop density other than to note a high density of 'black spot' damage was visible. However, they did report a bubble density on the order of 6×10^{23} m^{-3}, again higher than measured in this study. They estimated the average diameter of their bubbles to be around 1 nm.

It is significant to note that the Fujii and Foster studies saw a higher density of nano-cavities than observed in the current study but at smaller sizes. The two counterbalancing factors taken together tend to reduce the apparent difference in cavity volume. It should be noted that neither Fujii nor Foster reported seeing any significant amount of bubbles on the grain boundaries, but it does not appear that grain boundaries were examined with a level of scrutiny comparable to that of the current study.

Garner and Toloczko also reported small cavities observed at 2–6 dpa in a Russian stainless fuel pin tubes extracted from a PWR-type reactor used to simulate submarine cores [17]. The sizes were larger, however than those of the current study, 5–11 nm, and the concentrations were lower at 3 to 23×10^{20} m^{-3}.

There is another potential consequence of the strong development of nano-cavity microstructure and concurrent acceleration of hydrogen storage. It has been proposed that significant levels of void swelling will occur in austenitic components of PWR internals when irradiated to high neutron exposures [18] and small amounts of swelling were found in a PWR baffle bolt irradiated at 320–333 °C [19]. It is not certain, however, whether the nano-cavities observed in this study represent the onset of void swelling since the temperatures of this thimble are near the lower-temperature limit (~300 °C) of swelling in austenitic steels [20]. Voids have been observed at PWR-relevant dpa rates in various Russian stainless steels irradiated in several fast reactors at temperatures as low as 320 °C and sometimes as low as 280 °C [20–25].

It is well known that helium bubbles can serve as nuclei for voids so it possible that the nano-cavities observed in this study at 70 dpa may presage the onset of swelling at higher doses anticipated for extended PWR operation to 60 years.

However, it is the strong association of nano-cavities on grain boundaries seen in this study that is of more concern in the near term. Previous studies at lower exposures have generally not found a strong association, leading to the conclusion that this observation might represent the development of a new stage of microstructural evolution that requires critical amounts of helium to have accumulated before hydrogen storage on grain boundaries can occur. Additional studies are required to determine if grain boundary nano-cavity association is an inevitable consequence of increasing neutron exposure.

5. Conclusions

Transmission electron microscopy has been used to examine the microstructure of a 316SS flux thimble from an operating PWR. In the range of 33–70 dpa and 290–315 °C the original cold-worked dislocation network had completely disappeared and was replaced by fine dispersions of Frank loops and small nano-cavities at very high densities. The latter appear to be bubbles containing high levels of helium and hydrogen. Cavities at grain boundaries may promote IG failure and increase susceptibility to IGSCC. The possibility also exists that these nano-cavities presage the development of significant void swelling at doses above 70 dpa.

Earlier it was predicted that significant amounts of hydrogen in excess of that predicted by Sievert's Law would be stored when sufficient helium-nucleated cavities were formed in irradiated stainless steels. It appears that this prediction is supported by the data presented in this paper. Comparison of our results with those of comparable studies on thimble tubes irradiated to lower exposures shows that hydrogen storage increases dramatically as nano-cavities begin to dominate the microstructure.

Acknowledgements

This research was supported by the Office of Nuclear Energy, Science and Technology, US Department of Energy, under Contract DE-AC06-76RLO 1830. Additional support was provided by Vattenfall AB Ringhals and by the Cooperative IASCC research project through EPRI. Pacific Northwest National Laboratory is operated for the US DOE by Battelle Memorial Institute.

References

[1] H.-T. Tang, J.D. Gilreath, Fontevraud 5, Contribution of Materials Investigation to the Resolution of Problems Encountered in Pressurized Water Reactors, Fontevraud, France, 2002, p. 322.
[2] D.J. Edwards, E.P. Simonen, S.M. Bruemmer, P. Efsing, in: Proceedings of 12th International Conference on Environmental Degradation of Materials in Nuclear Power System – Water Reactors, 2005, p. 419.
[3] K. Fujimoto, T. Yonezawa, E, Wachi, Y. Yamaguchi, M. Nakano, R.P. Shogan, J.P. Massoud, T.R. Mager, in: Proceedings of 12th International Conference on Environmental Degradation of Materials in Nuclear Power System – Water Reactors, 2005, p. 299.
[4] J. Conermann, R. Shogan, K. Fujimoto, T. Yonezawa, Y. Yamaguchi, in: Proceedings of 12th International Conference on Environmental Degradation of Materials in Nuclear Power System – Water Reactors, 2005, p. 277.
[5] F.A. Garner, W.G. Wolfer, H.R. Brager, in: International Symposium on Effect of Radiation on Structural Materials ASTM STP 683, 1978, p. 160.
[6] F.A. Garner, D.S. Gelles, J. Nucl. Mater. 159 (1988) 286.
[7] Research Report No. TUO73-043631, VTT Technical Research Centre of Finland, 2004.
[8] K. Fujii, K. Fukuya, G. Furutani, T. Torimaru, A. Kohyama, Y. Katoh, in: 10th International Symposium on Environmental Degradation of Materials in Nuclear Power Systems – Water Reactors, The Minerals, Metals and Materials Society, Pennsylvania (2002) CD format, no page numbers.
[9] A.J. Jacobs, in: F.A. Garner, C.H. Henager Jr., N. Igata (Eds.), Influence of Radiation on Material Properties: 13th International Symposium (Part II) ASTM STP 956, 1987, p. 239.
[10] F.A. Garner, L.R. Greenwood, in: 11th International Conference on Environmental Degradation of Materials in Nuclear Power Systems – Water Reactors, 2003, p. 887.
[11] F.A. Garner, E.P. Simonen, B.M. Oliver, L.R. Greenwood, M.L. Grossbeck, W.G. Wolfer, P.M. Scott, J. Nucl. Mater. 356 (2006) 122.
[12] L.R. Greenwood, J. Nucl. Mater. 115 (1983) 137.
[13] L.R. Greenwood, F.A. Garner, J. Nucl. Mater. 233–237 (1996) 1530.
[14] F.A. Garner, L.R. Greenwood, B.M. Oliver, in: R.K. Nanstad, M.L. Hamilton, F.A. Garner, A.S. Kumar (Eds.), Effects of Radiation on Materials: 18th International Symposium, ASTM STP 1325, American Society of Testing and Materials, 1999, p. 794.
[15] K. Fukuya, K. Fujii, M. Nakano, N. Nakajima, in: Proceedings of the Tenth International Symposium on Environmental Degradation of Materials in Nuclear Power Systems - Water Reactors, Lake Tahoe, NV. August 5–9, 2001, CD format, no page numbers.
[16] J.P. Foster, D.L. Porter, D.L. Harrod, T.R. Mager, M.G. Burke, J. Nucl. Mater. 224 (1995) 207.
[17] F.A. Garner, M.B. Toloczko, J. Nucl. Mater. 251 (1997) 252.
[18] F.A. Garner, L.R. Greenwood, D.L. Harrod, in: Proceedings of the Sixth International Symposium on Environmental Degradation of Materials in Nuclear Power Systems - Water Reactors, San Diego, CA. August 1–5, 1993, p. 783.
[19] D.J. Edwards, E.P. Simonen, F.A. Garner, L.R. Greenwood, B.M. Oliver, S.M. Bruemmer, J. Nucl. Mater. 317 (2003) 32.
[20] S.I. Porollo, Yu V. Konobeev, A.M. Dvoriashin, A.N. Vorobjev, V.M. Krigan, F.A. Garner, J. Nucl. Mater. 307–311 (2002) 339.
[21] O.P. Maksimkin, K.V. Tsai, L.G. Turubarova, T. Doronina, F.A. Garner, J. Nucl. Mater. 329–333 (2004) 625.
[22] O.P. Maksimkin, K.V. Tsai, L.G. Turubarova, T.A. Doronina, F.A. Garner, J. Nucl. Mater. 367–370 (2007) 990.
[23] V.S. Neustroev, V.K. Shamardin, Z.E. Ostrovsky, A.M. Pecherin, F.A. Garner, in: M.L. Hamilton, A.S. Kumar, S.T. Rosinski, M.L. Grossbeck (Eds.), Effects of Radiation on Materials: 19th International Symposium, ASTM STP 1366, American Society for Testing and Materials, 2000, p. 792.
[24] F.A. Garner, D.J. Edwards, S.M. Bruemmer, S.I. Porollo, Yu V. Konobeev, V.S. Neustroev V.K. Shamardin, A.V. Kozlov, in: Fontevraud 5 Symposium on Contribution of Materials Investigation to the Resolution of Problems Encountered in Pressurized Water Reactors, Fontevraud, France, 2002, pp. 393.
[25] F.A. Garner, S.I. Porollo, Yu V. Konobeev, V.S. Neustroev, O.P. Maksimkin, in: Fontevraud 6 Symposium on Contribution of Materials Investigations to Improve the Safety and Performance of LWRs, Fontevraud, France, 2006, p. 637.